



ELSEVIER

Surface Science 366 (1996) 149–165

surface science

## ToF-SIMS study of alternate polyelectrolyte thin films: Chemical surface characterization and molecular secondary ions sampling depth

A. Delcorte <sup>a,\*</sup>, P. Bertrand <sup>a</sup>, X. Arys <sup>b</sup>, A. Jonas <sup>b</sup>, E. Wischerhoff <sup>c</sup>, B. Mayer <sup>c</sup>,  
A. Laschewsky <sup>c</sup>

<sup>a</sup> *Unité de Physico-Chimie et de Physique des Matériaux, Université Catholique de Louvain, 1 Place Croix du Sud,  
B-1348 Louvain-la-Neuve, Belgium*

<sup>b</sup> *Unité de Chimie et de Physique des Hauts Polymères, Université Catholique de Louvain, 1 Place Croix du Sud,  
B-1348 Louvain-la-Neuve, Belgium*

<sup>c</sup> *Département de chimie, Université Catholique de Louvain, 1 Place Croix du Sud, B-1348 Louvain-la-Neuve, Belgium*

Received 23 February 1996; accepted for publication 23 April 1996

---

### Abstract

Multilayered assemblies of alternate polyelectrolytes have been synthesized by dipping charged silicon wafers successively into solutions of polyelectrolytes of opposite charge. In this study, three types of assemblies and several thicknesses are investigated by Time-of-Flight Secondary Ion Mass Spectrometry (ToF-SIMS), in combination with other characterization techniques ( X-Ray Photoelectron Spectroscopy (XPS), X-Ray Reflectivity (XRR) and Atomic Force Microscopy (AFM) ).

The sensitivity of ToF-SIMS to the extreme surface provides a powerful tool to verify the chemical structure, as well as the spatial homogeneity of the topmost layers. Monolayers of complex polyelectrolytes differing only by the end of the pendant group or by the monomer chain length can be distinguished easily, notwithstanding the interference with the information coming from the underlying layers. The chemical imaging capability of ToF-SIMS allows the identification of the defects and contaminants in the surface layer, as well as the verification of the thickness uniformity at a local scale ( $\sim 1 \mu\text{m}$ ). In addition, the proof of a regular build-up is given by the disappearance of the substrate signal ( $\text{Si}^+$ ) when the number of layers increases.

On the other hand, the question of the information depth in ToF-SIMS, which constitutes an important issue for the characterization of very thin films, is addressed. The attenuation depth in the organic film is determined for atomic and molecular secondary ions ( $\text{Si}^+$ ,  $\text{SiOH}^+$ ,  $\text{SiO}_3\text{H}^-$ ), mainly by the correlation with XPS and XRR data. The decay of the mean emission depth when the ion size increases makes the largest molecular ions the most surface sensitive.

**Keywords:** Adhesion; Coatings; Ion Emission; Polyelectrolyte; Secondary Ion Mass Spectroscopy; Self-Assembly; X-Ray Photoelectron Spectroscopy; X-Ray Reflectivity

---

\* Corresponding author. Fax: +32 10 473452; e-mail: delcorte@pcpm.ucl.ac.be

## 1. Introduction

Multilayered assemblies alternating polycationic and polyanionic layers have been developed recently [1–4]. They are built up by dipping a charged substrate alternately into solutions of polyelectrolytes bearing opposite charges. In this way, the surface polarity is reversed after each deposition step, and the electrostatic attraction between the polyelectrolytes in solution and the charged surface at the following step is ensured. In most cases, the assemblies are characterized by macroscopic techniques (UV/VIS spectroscopy, quartz crystal microbalance and X-Ray Reflectivity [2–4]), and rarely by microscopic probes. This lack of investigation at a microscopic scale is problematic, keeping the monolayer character of the coatings in mind. Moreover, information on the microscopic interactions is desirable. In this work, ToF-SIMS is used in combination with other techniques (XPS, XRR, AFM) to characterize polyelectrolyte assemblies. The ability of ToF-SIMS to provide valuable information concerning the chemical structure of the extreme surface is well known and the interest of this technique for the analysis of very thin films has already been proven [5–8]. In addition, the correlation with data obtained from other characterization techniques gives a better understanding of the secondary ion emission processes, and shows, moreover, that quantitative ToF-SIMS can be achieved.

## 2. Experimental

### 2.1. Samples

#### 2.1.1. Polyelectrolytes

The polyelectrolytes used for the multilayer buildup in this study are listed in Table 1 [4,9]. The polyelectrolytes (6,7) are commercial products (Aldrich) whereas the polycations (1–5) were synthesized in the Dept. of Chemistry of the university. Their synthesis will be described elsewhere [10].

#### 2.1.2. Multilayered assemblies

Silicon wafers were used as supports for the multilayered assemblies. They were cleaned into a

$\text{H}_2\text{SO}_4/\text{H}_2\text{O}_2$  (35%) 1:1 solution at 80°C for 20 min and negative charges were created on the surface by keeping the wafers into a  $\text{H}_2\text{O}_2$  (35%)/conc. $\text{NH}_4\text{OH}/\text{H}_2\text{O}$  1:1:5 solution at 80°C for 20 min. For all assemblies, a buffer polyelectrolyte bilayer was realized by dipping the treated substrates first into a solution of polyelectrolyte (6), then into a solution of polyelectrolyte (7). In principle, the deposition of a thin layer of polyelectrolyte (6) onto the treated silicon was ensured by the electrostatic attraction between the opposite charges of the substrate and the polyelectrolyte. As the sample surface polarity was reversed by the deposition of the polycation (6), the following layer consisting of the polyanion (7) could be easily adsorbed by the same mechanism. The assemblies of alternate polyelectrolytes (6)/{(7)/(3)}<sub>x</sub> were obtained by dipping the assembly (6)/(7) successively into solutions of polycation (3) and polyanion (7) [4].

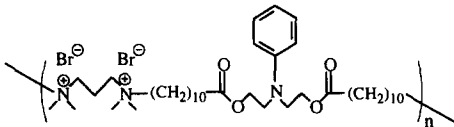
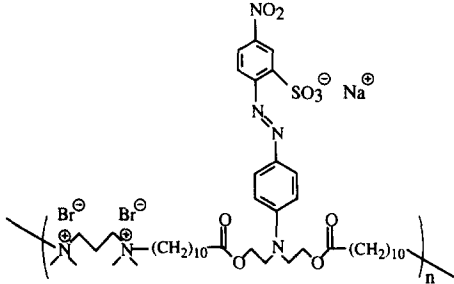
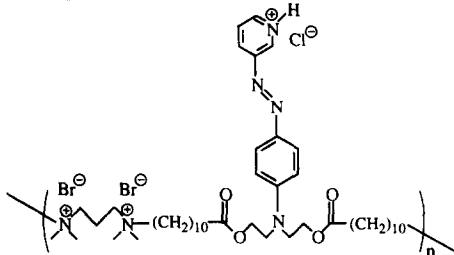
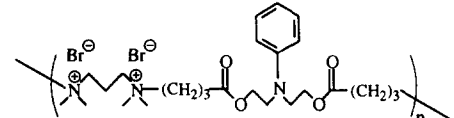
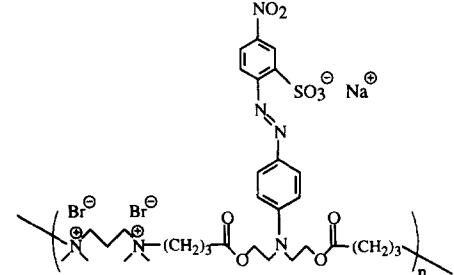
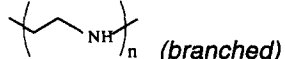
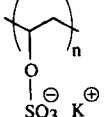
The assemblies involving the polyelectrolytes (1,2,4,5) were realized in a different way, by the new CoMPAS coating technique [9]. First, the substrate already bearing the buffer bilayer (6)/(7) was dipped into a solution of polyelectrolyte (1) or (4). In the following step, the surface layer of polyelectrolyte (1) or (4) was activated in order to obtain polyampholyte (2) or (5), reversing the sign of the surface charge, and allowing the deposition of a new layer of polycation (1) or (4). During the activation step, the aniline residue of polycation (1) or (4) was converted into an anionic azo dye by coupling at the surface with the diazonium salt derived from sodium 2-amino-5-nitrobenzene-sulfonate. The formulation of the final assembly was then (6)/(7)/(2 or 5)<sub>x</sub> or (6)/(7)/(2 or 5)<sub>x-1</sub>/(1 or 4), depending on whether the last operation was an activation or a deposition step. The concentration of the polyelectrolyte solutions used in this work was  $2 \times 10^{-2}$  M.

### 2.2. Characterization techniques

#### 2.2.1. ToF-SIMS

The system consists of a Time-of-Flight SIMS microprobe-microscope (Charles Evans and assoc.) using a (5 kHz) pulsed  $\text{Ga}^+$  beam (15 kV, 400 pA DC) [11]. The  $\text{Ga}^+$  beam is rastered over a 97 x

Table 1  
Formulae of the polyelectrolytes used for the multilayered assemblies

Polyelectrolyte	Chemical Formula
(1)	
(2)	
(3)	
(4)	
(5)	
(6)	
(7)	

97  $\mu\text{m}^2$  area. The secondary ions are accelerated by a 3 kV voltage immediately after emission and deflected by three electrostatic analyzers in order to compensate their initial energy and angular distributions. The result of this is a high mass resolution ( $M/\Delta M > 5000$  at mass 28 D), allowing the discrimination of secondary ions with the same nominal mass. The mass spectrum is obtained by measuring the time-of-flight distribution of the ions from the sample surface to the detector. The total ion fluence for one spectrum acquisition is  $10^{12}$  ions  $\text{cm}^{-2}$ , which is known to ensure static conditions in the case of polymer samples [12]. For the data processing, two normalization procedures are used. The data related to the substrate ions are normalized to the total spectrum intensity (Figs. 3 and 6, inset in Fig. 7), except when absolute intensities are required to determine accurate emission depths by the comparison between SIMS and XPS data (Figs. 7 and 8). The normalization by the total spectrum intensity cannot be used for the comparison of different polyelectrolytes, due to the very large variation of the dominant substrate signal, depending on the film thickness. For this purpose, a normalization involving ions sputtered from the organic film which are rather insensitive to the thickness of the assemblies is needed. In order to evidence the correct variation, the peak intensities are then divided by the intensity of an uncharacteristic hydrocarbon peak (Table 4:  $\text{C}_2\text{H}_3^+$  in the positive mode and  $\text{CH}^-$  in the negative mode) or by the intensity of a chosen characteristic peak (Table 5:  $\text{C}_3\text{H}_8\text{N}^+$ ).

### 2.2.2. XPS

The XPS equipment was a SSI-X-Probe (SSX-100/206 from Fisons) [13,14] with an aluminum anode (10 kV, 11.5 mA) and a quartz monochromator. The photoelectrons were energy-discriminated by a hemispherical analyzer and detected by a micro-channel plate. The angle of detection in the usual configuration was  $35^\circ$  with respect to the sample surface. The analyzed surface was a spot of  $1000 \mu\text{m}$ . For this study, detailed scans of the main lines of each element found in the polyelectrolyte formulations were recorded. Measurements at different detection angles ( $15^\circ$ ,

$25^\circ$ ) were performed with a sample holder rotating around the three axes.

### 2.2.3. XRR

The X-Ray Reflectivity measurements were performed with a Siemens D5000 diffractometer for incidence angles lower than  $4.5^\circ$ , using Cu  $\text{K}_\alpha$  radiation and a secondary graphite monochromator. A good collimation of the beam was achieved by placing a knife edge a few  $\mu\text{m}$  above the sample surface. The data were corrected for background scattering and variation of the illuminated area at very low angles of incidence. For the samples studied in this paper, the data were analyzed by fitting a model consisting of a succession of thin sublayers on flat substrates, using a matrixial iteration formalism derived from Fresnel's equations, except for samples containing polyelectrolyte (3), where the thickness was simply deduced from the spacing of the Kiessig fringes.

### 2.2.4. AFM

AFM analyses were performed in air on an Autoprobe<sup>TM</sup> CP from Park Scientific Instruments (Sunnyvale, CA). In order to avoid film degradation due to the tip, they were carried on in the non-contact mode with Ultralevers having stiffnesses of about  $15 \text{ N m}^{-1}$ . A  $100 \mu\text{m}$  scanner was used and the scanning speed was typically equal to  $10 \mu\text{m sec}^{-1}$ . The film thickness was evaluated by measuring on a flattened image the difference between the mean height of a region on the film and that of a region of the same area on the silicon substrate revealed by a scratch.

## 3. Results and discussion

Three types of assemblies and several thicknesses have been characterized, each of them by two techniques at least. These assemblies and the analyses performed are listed in Table 2 for clarity. A first characterization of the samples by macroscopic techniques (UV/VIS spectroscopy, colours, optical microscopy) demonstrated their homogeneity at this scale.

Table 2  
Different characterization techniques used for the analysis of the multilayered assemblies

Multilayer assembly	ToF-SIMS	XPS/ARXPS*	XR reflectivity	AFM
bare silicon	X	X*	X	
(6)	X	X		
(6)/(7)	X	X	X	
(6)/(7)/(1)	X	X		
(6)/(7)/(2)	X	X	X	
(6)/(7)/(2) <sub>2</sub>	X	X/X*	X	
(6)/(7)/(2) <sub>3</sub>	X	X*		
(6)/(7)/(2) <sub>4</sub>	X	X		
(6)/(7)/(3)	X	X	X	
(6)/(7)/(3) <sub>2</sub>	X	X/X*	X	
(6)/(7)/(3) <sub>3</sub>	X	X	X	
(6)/(7)/(3) <sub>4</sub>	X	X	X	
(6)/(7)/(4)	X			
(6)/(7)/(4) <sub>2</sub>	X			X

### 3.1. ToF-SIMS characterization of the topmost layers

Fig. 1a shows the positive secondary ion mass spectrum of the assembly (6)/(7)/(1). The most intense peak in the spectrum corresponds to Si<sup>+</sup> (28 D), suggesting that the silicon substrate is not completely covered or/and that the thickness of the multilayer assembly is not sufficient to mask the substrate ion emission. This point will be discussed in detail in Section 3.2. Characteristic nitrogen-containing ions also appear at even masses (58 D, 84 D, 98 D, 104 D, 120 D, 132 D, 146 D) whereas hydrocarbon ions appear at odd masses (41 D, 55 D, 77 D). In polyelectrolyte (1), two main series of ions must be distinguished (Table 3): the main chain (MC) produces rather saturated ions containing at least one nitrogen atom whereas the pendant group (PG) produces unsaturated ions containing at least one phenyl. Most of these ions are also emitted from polyelectrolytes (2–5) but with different intensities, as shown below.

The negative spectrum of the assembly (6)/(7)/(1) (Fig. 1b) also shows interesting features above 30 D. Peaks corresponding to the intermediate polyanion layer or to the counterions of the polycation (1) layer exhibit significant intensities: Br<sup>-</sup> (two isotopes at 79 and 81 D) is the counterion of

polyelectrolyte (1) whereas the SO<sub>x</sub>H<sub>y</sub><sup>-</sup> series (64, 80 and 97 D) corresponds to the pendant group of polyelectrolyte (7). This raises once more the two questions concerning the coverage uniformity and the secondary ion (SI) information depth in the case of organic films, which will be addressed further (Section 3.2).

As shown in Table 1, the formulae of the polyelectrolytes (1–5) exhibit many common features and few differences. Nevertheless, the sensitivity of the ToF-SIMS to the chemical functionalities of the extreme surface allows the identification of these polyelectrolytes. Two effects are examined below, the sensitivity both to the pendant group and to the length of the alkyl chain contained in the polymer backbone. On the other hand, the spatial homogeneity of the layers will be verified by imaging the surface and the regular build-up by monitoring the decay of the substrate signal.

#### 3.1.1. Sensitivity to the pendant group

The values of the sum of the MC and PG peak intensities are listed in Table 4 for the assemblies (6)/(7)/(1), (6)/(7)/(2) and (6)/(7)/(3).  $\sum$ PG is decreasing when going from polyelectrolyte (1) to (3), which indicates a lower ability to produce these ions from polyelectrolytes (2,3). This can be easily explained by the chemistry of the polyelectrolytes. Indeed, one more bond must be broken in polyelectrolytes (2,3) to emit the so-called PG ions. As the difference between polyelectrolytes (1–3) lies in the pendant group only, one would expect a constant intensity for the MC peaks. Table 4 shows that this is not the case: the sum of the MC peak relative intensities is decreasing, too, when going from polyelectrolyte (1) to (3). This can be explained by a masking of the main chain by the pendant group, which is increased in the cases of polyelectrolytes (2,3). This observation shows the sensitivity of ToF-SIMS to the organization of the polyelectrolyte top layer. Moreover, the fact that  $\sum$ PG decreases more strongly than  $\sum$ MC is in favor of a real fixation of the additional functionality on the pendant phenyl group of polyelectrolyte (1). The  $\sum$ MC and  $\sum$ PG values given in Table 4 suggest that the activation of polyelectrolyte (1), realized “on the layer” in order to obtain

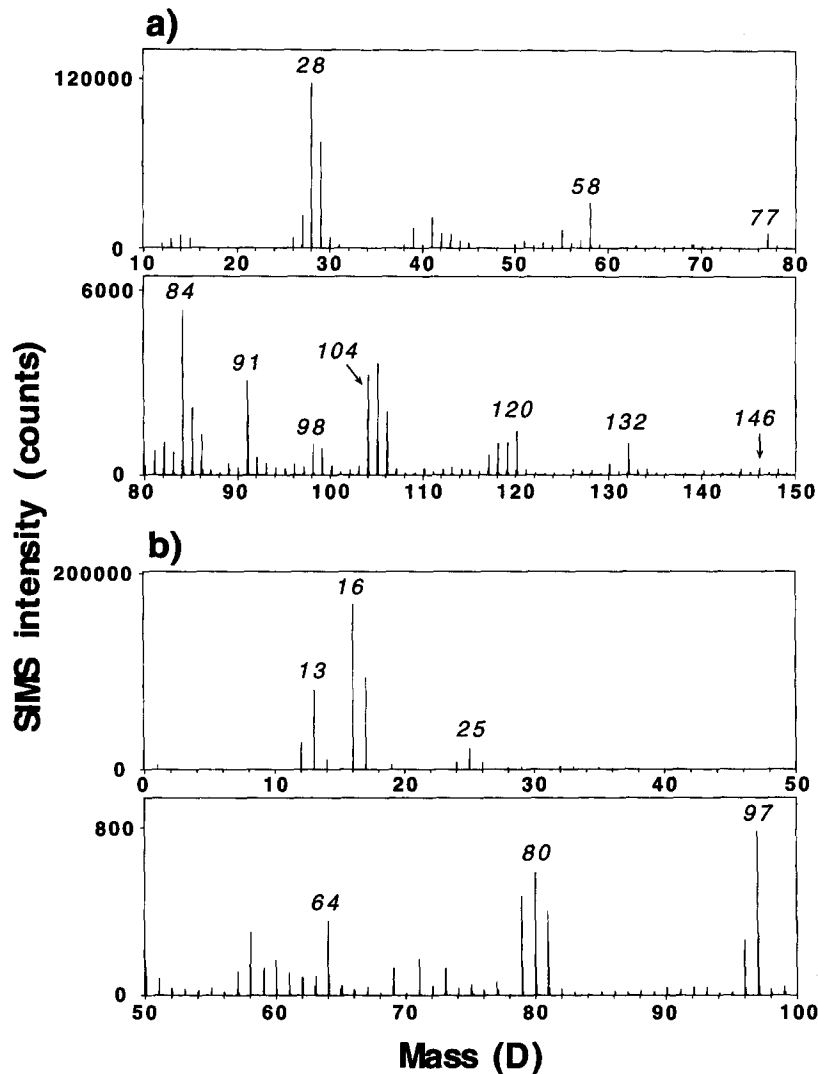


Fig. 1. Positive (a) and negative (b) SI mass spectra of the assembly (6)/(7)/(I).

polyampholyte (2), is less efficient than the activation realized prior to deposition, used to obtain polyelectrolyte (3). Another interpretation may involve a difference of organization of the polycation at the surface.

Direct indications of the successful activation of

polyelectrolyte (I) in the adsorbed layer in order to obtain polyampholyte (2) in situ can be found in the negative spectrum of these species. Characteristic fragments of the functional group appear at masses 46, 137 and 216 D. They were attributed to the following ions:

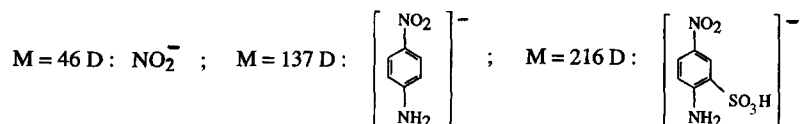


Table 3

Formulae of the main characteristic ions observed in the positive SI mass spectrum of polyelectrolyte (*I*). The ion mass is indicated in daltons (D)

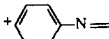
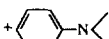
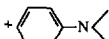
Main Chain (MC)		Pendant Group (PG)	
	M = 58 D		M = 77 D
	M = 84 D		M = 104 D
	M = 98 D		M = 120 D
	M = 112 D		M = 132 D
	M = 126 D		
	M = 140 D		

Table 4

Characteristic indicators of polyelectrolytes (*I*–*3*);  $\sum MC$  is the sum of the peak areas corresponding to the main chain of polyelectrolyte (*I*);  $\sum PG$  is the sum of the peak areas corresponding to the pendant group of polyelectrolyte (*I*); every indicator is based on normalized SI peak areas (see Section 2.2.1); the standard deviation is <5% of the indicated values, except in the case of  $\sum MC((6)/(7)/(I))$ , where it reaches 10% of the indicated value

	(6)/(7)/(I)	(6)/(7)/(2)	(6)/(7)/(3)
Positive ions			
$\sum MC$	2.0	1.24	1.39
$\sum PG$	$79 \times 10^{-2}$	$28 \times 10^{-2}$	$7.9 \times 10^{-2}$
$\sum PG/\sum MC$	$40 \times 10^{-2}$	$23 \times 10^{-2}$	$5.7 \times 10^{-2}$
peak 78 D/peak 77 D	0.20	0.21	1.27
Negative ions			
peak 46 D ( $NO_2^-$ )	$3.0 \times 10^{-3}$	$29 \times 10^{-3}$	$9.6 \times 10^{-3}$
peak 137 D	$1.4 \times 10^{-4}$	$10 \times 10^{-4}$	$1.4 \times 10^{-4}$
peak 216 D	$2.0 \times 10^{-5}$	$83 \times 10^{-5}$	$15 \times 10^{-5}$
peak 80 D ( $SO_3^-$ )	$9.1 \times 10^{-3}$	$15 \times 10^{-3}$	$12 \times 10^{-3}$
peak 97 D ( $SO_4H^-$ )	$16 \times 10^{-3}$	$6.1 \times 10^{-3}$	$7.4 \times 10^{-3}$

Table 4 gives their characteristic values for polyelectrolytes (*I*–*3*). The drastic increase of the intensities of peaks at 46, 137 and 216 D when going from polyelectrolyte (*I*) to (*2*) is in favor of an activation which is at least partial. On the other hand, the presence of the  $SO_xH_y^-$  ions in the negative spectrum of the assembly (6)/(7)/(I) shows that these ions cannot be used as a fingerprint of polyampholyte (*2*). Nevertheless, the evolution of these ion intensities, when activating polyelectro-

lyte (*I*) to obtain polyampholyte (*2*), reveals interesting features. Table 4 shows that the intensity of the  $SO_3^-$  ion (80 D) increases slightly whereas the intensity of the  $SO_4H^-$  ion (97 D) is reduced by a factor of nearly 3 when going from polyelectrolyte (*I*) to (*2*). As  $SO_4H^-$  cannot be sputtered from the activated polycation layer without recombination (the end of the pendant group is a  $-SO_3^-$ ), this ion must be exclusively attributed to the polyelectrolyte (*7*) layer. This leads to two conclusions: (i) the increase of the  $SO_3^-$  ion intensity, accompanied by the drastic decrease of the  $SO_4H^-$  ion intensity, is a significant proof of activation. Indeed, if the  $SO_3^-$  ion was only due to the polyelectrolyte (*7*) layer, its intensity should be similarly reduced. (ii) The decay of the  $SO_4H^-$  ion intensity shows that the activated polyampholyte (*2*) layer is thicker or more complete than the initial polyelectrolyte (*I*) layer.

The functionalization leading to polyelectrolyte (*3*) can also be directly evidenced by comparing peak intensities. As the pendant group of polyelectrolyte (*3*) bears a pyridine residue, it should be very easy to chose the characteristic ion  $C_5H_4N^+$  (78 D) as an indicator of its presence on the surface. Unfortunately, it is not sufficiently mass-separated from the isobar  $C_6H_6^+$  to be extracted alone. To avoid this problem, we report in Table 4 the ratio (peak 78 D/peak 77 D) which is expected to be constant for every polyelectrolyte except (*3*). This ratio is nearly six times greater for polyelectrolyte (*3*), which confirms our expectations.

### 3.1.2. Sensitivity to the length of the alkyl chain contained in the polymer backbone

Polyelectrolytes (1) and (4) exhibit very similar secondary ion mass spectra as, being homologues, they are close to each other from the chemical viewpoint. However, differences in the main chain peak intensities are expected. Indeed, polyelectrolyte (1) is able to produce main chain fragments ( $C_xH_yN^+$ ) containing up to 14 carbon atoms, whereas polyelectrolyte (4) cannot give saturated  $C_xH_yN^+$  ions with more than 7 carbon atoms without recombination. The difference in the alkyl spacer length should then be evidenced by the comparison of the main chain peak intensities between these two polyelectrolytes. Table 5 lists the intensity of the main chain peaks, normalized by the intensity of the peak  $C_3H_8N^+$ , for the two assemblies (6)/(7)/(1) and (6)/(7)/(4). The last column indicates for each peak the ratio between the values related to the two assemblies (column A divided by column B). These ratios show that the peak  $C_5H_{10}N^+$  (84 D) is as intense in the two assemblies (with reference to peak 58 D). The loss of intensity of the main chain peaks in polyelectrolyte (4) is marked for the peak  $C_6H_{12}N^+$ , and the intensity decreases more and more for the peaks  $C_xH_yN^+$  with  $x > 6$ . The  $x$  value for which the intensity falls in polyelectrolyte (4) does not give an absolute value of the alkyl spacer length, as the main intensity loss occurs between  $x = 5$  and  $x = 6$ . Nevertheless, the drastic relative decrease of the  $C_xH_yN^+$  ion intensity in polyelectrolyte (4) with increasing  $x$  is significant for the difference in the length of the alkyl spacer. The ratio (peak 58

D/peak 77 D), equal to 3.6 for polyelectrolyte (1) and to 3.0 for polyelectrolyte (4), gives also a qualitative indication concerning the alkyl spacer length. Indeed, the more pronounced screening of the main chain in polyelectrolyte (4) is consistent with a shorter repeat unit of the polymer. This result demonstrates that apparently small changes in the chain structure of the polyelectrolytes give rise to marked effects in their organization within the coating.

### 3.1.3. Chemical mapping of the surface

As the deposition technique allows the design of polyelectrolyte layers at the molecular scale (10 Å thickness), it is very important to verify the quality of the surface layer, i.e. its chemical homogeneity at a local scale (incomplete coverage, defects, contamination). The control of the local quality of the layers is useful not only for future applications, but also for the understanding and development of the deposition process itself. In ToF-SIMS, it is possible to obtain a chemical mapping of the extreme surface, with a fairly good spatial resolution ( $\sim 1 \mu\text{m}$ ). The capability of ToF-SIMS to verify the homogeneity of very thin layers has already been demonstrated with Langmuir-Blodgett films [8].

Fig. 2 shows four images obtained from an imperfect assembly (6)/(7)/(3). This constitutes an exceptional case, but it reveals valuable informations concerning the application of ToF-SIMS to very thin multilayered assemblies. Fig. 2a and b (positive ions) correspond exactly to the same area. Fig. 2c and d (negative ions) are slightly moved and distorted in comparison with Fig. 2a and b, as indicated by the bright circle. Fig. 2a is a mapping of the ion  $C_3H_8N^+$ , which is characteristic of the main chain of polyelectrolyte (3). The image of the ion  $C_3H_8N^+$  looks homogeneous. However, the image of the  $Si^+$  substrate ion is strongly inhomogeneous (Fig. 2b, showing a dispersion of dark circles (5  $\mu\text{m}$  diameter) into a continuous bright phase. In the negative mode, inhomogeneities are also observed: Fig. 2c and d respectively show the spatial distribution of the ( $Cl^- + Br^-$ ) and  $O^-$  ions. Chlorine and bromine are the counterions of polyelectrolyte (3), whereas oxygen comes mainly from the substrate. The contrast on the chlorine

Table 5

Comparison between polyelectrolyte (1) and polyelectrolyte (4); the peak intensities in the two first columns are normalized to peak 58 D ( $C_3H_8N^+$ ); the assignment of the peaks is reported in Table 3; the standard deviation is <20% of the indicated values

MC peaks	A:(6)/(7)/(1)	B:(6)/(7)/(4)	A/B
peak 58 D	1.0	1.0	1.0
peak 84 D	$1.7 \times 10^{-1}$	$1.7 \times 10^{-1}$	1.05
peak 98 D	$3.1 \times 10^{-2}$	$1.7 \times 10^{-2}$	0.56
peak 112 D	$1.0 \times 10^{-2}$	$0.56 \times 10^{-2}$	0.53
peak 126 D	$0.69 \times 10^{-2}$	$0.29 \times 10^{-2}$	0.43
peak 140 D	$0.61 \times 10^{-2}$	$0.20 \times 10^{-2}$	0.33

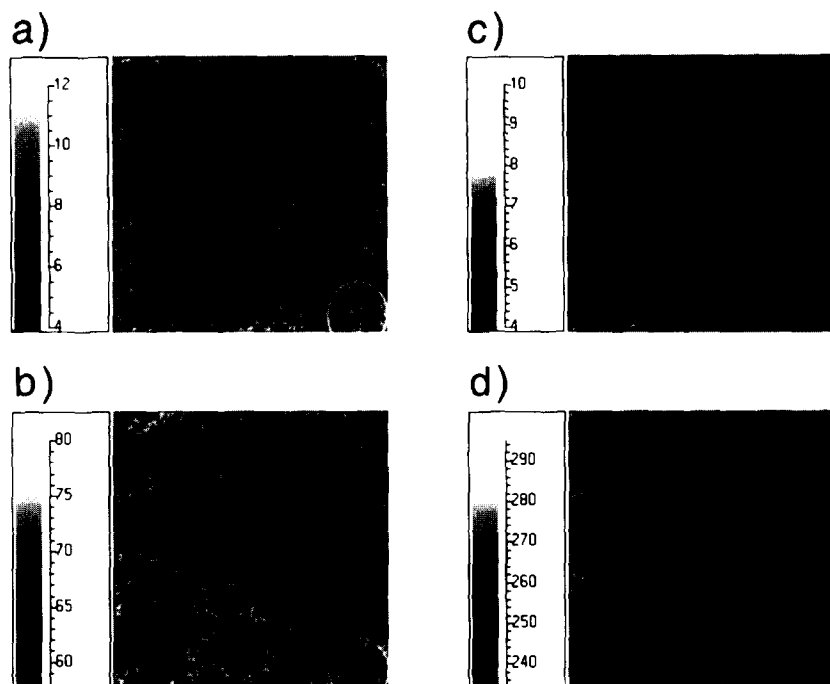


Fig. 2. Chemical imaging of an imperfect assembly (6)/(7)/(3). Images (a) to (d) show respectively the distribution of the  $C_3H_8N^+$ ,  $Si^+$ ,  $Cl^-$  and  $O^-$  ions on the surface. The field of view is approximately  $50 \times 50 \mu m^2$ . The bright circle indicates the same defect in the four images.

image is less clear than on the oxygen one. Nevertheless, it seems that a high chlorine intensity is observed where oxygen is depleted (bright circle in Fig. 2c and d). These images can be interpreted as follows: polyelectrolyte (3) covers the whole area (Fig. 2a) but the thickness of the organic layer varies from place to place, masking more or less the substrate signals (Fig. 2b and d). The fact that the contrast on  $C_3H_8N^+$  is weak compared to the contrast on silicon and oxygen is probably related to different emission depth for atomic and molecular ions (see Section 3.2.) As  $C_3H_8N^+$  is sputtered from the extreme surface, one complete monolayer of polyelectrolyte (3) is enough to obtain the saturation of this ion intensity, whereas the attenuation of the  $Si^+$  and  $O^-$  signals needs several monolayers. The (chlorine + bromine) image, also corresponding to polyelectrolyte (3) is in agreement with this interpretation: indeed, the contrast on chlorine and bromine is strong compared to the contrast on  $C_3H_8N^+$ , which may be explained by a greater emission depth for these atomic ions, resulting in

a higher intensity where the polyelectrolyte (3) layer is thicker.

The presence of both  $Cl^-$  and  $Br^-$  ions is noteworthy, as the question has been raised whether the polyelectrolyte complex formation at the surface is quantitative or not. In the case of quantitative complexation, low molar mass counterions such as  $Cl^-$  and  $Br^-$ , should be absent. For the system studied, ToF-SIMS gives evidence that this is not the case, thus supporting studies on coatings made from poly(allylamine) and poly(styrene sulfonate) for which the presence of low molar mass counterions was inferred indirectly from the extent of X-ray absorption [2].

#### 3.1.4. Effect of the multilayer build-up

As observed in the preceding sections, the signal of the substrate atoms may be intense even with three polyelectrolyte layers (Fig. 1). The fundamental reason for this, i.e. the significant sampling depth of the atomic secondary ions, will be investigated in detail in Section 3.2. From the practical

viewpoint, this phenomenon allows us to verify the regular increase of the multilayer assembly in the first steps of the deposition (below 10 layers). Fig. 3 shows the intensity of the  $\text{Si}^+$  ion as a function of the number of layers for the two systems  $(6)/(7)/(3)_x$  and  $(6)/(7)/(2)_x$ . The successful deposition of the buffer layers is not clear, when looking at the value of the  $\text{Si}^+$  intensity for the two first layers. By contrast, the  $\text{Si}^+$  signal begins to follow an exponential decay law with successive deposition of polyelectrolytes (2) or (3), in agreement with a constant increase of the sample thickness. As the polyelectrolytes are different in the two assemblies, the exact slope of the lines in Fig. 3 cannot be compared. Nevertheless, if we assume that the polyelectrolyte chains deposit parallel to the sample surface and that the pendant groups remain perpendicular to this surface, a bilayer of polyelectrolyte (2) should have a thickness of some 30 Å whereas the assembly (7)/(3) should be only 20 Å thick (according to the bond lengths). Fig. 3 suggests the inverse trend; the slope is much steeper for the assembly  $(6)/(7)/(3)_x$  than for the assembly  $(6)/(7)/(2)_x$ . As the thickness of the assembly (7)/(3) found by XRR is close to 20 Å, this implies that the polyelectrolyte (2) layers in the analyzed series  $(6)/(7)/(2)_x$  is either less complete, or that the arrangement is such that the pendant groups are

not perpendicular to the surface, resulting in a slower decay of the  $\text{Si}^+$  signal in ToF-SIMS.

### 3.2. Information depth in SIMS

An emission depth of 1 nm is often claimed in static SIMS. Unfortunately, few quantitative studies have been carried out in order to determine this information depth accurately in the case of organic materials [5–7]. In the course of this work, a knowledge of the emission depth of the substrate ions seemed of great interest for the evaluation of the layer quality. Moreover, it was important to know whether this emission depth was similar for atomic ( $\text{Si}^+$ ,  $\text{S}^-$ ) and molecular ions ( $\text{SiO}_3\text{H}^-$ ,  $\text{SO}_3^-$ ), in order to get a deeper understanding of our results. Two methods have been used to determine the emission depth of the substrate atoms: (i) A direct correlation between the SI intensities and the thickness of the multilayer assemblies (measured by X-Ray Reflectivity or Atomic Force Microscopy). The condition to get a significant relation between SIMS and XRR measurements is to have an homogeneous sample of limited roughness, whereas a correlation with AFM measurement can be achieved at a more local scale. (ii) A correlation between SIMS and XPS results. If an exponential decay as a function of depth is assumed for the secondary ion emission, as it is the case for photoelectrons in XPS [15], a linear relation binding SIMS and XPS data should be the consequence of a similar mean emission depth ( $\lambda$ ). This remains valid even if the sample thickness is not uniform, giving a powerful tool to estimate the SI information depths. Moreover, a linear correlation observed between different substrate SI peaks and the substrate photoelectron intensity measured at different angles of detection (ARXPS) would indicate a different SIMS emission depth for these ions. In this case, the condition of linearity is not affected by the roughness of the multilayer assembly, even for a low angle of detection in XPS, as long as the roughness amplitude is weak compared to the lateral characteristic dimension of the inhomogeneities. AFM measurements have shown that this condition was observed in our samples.

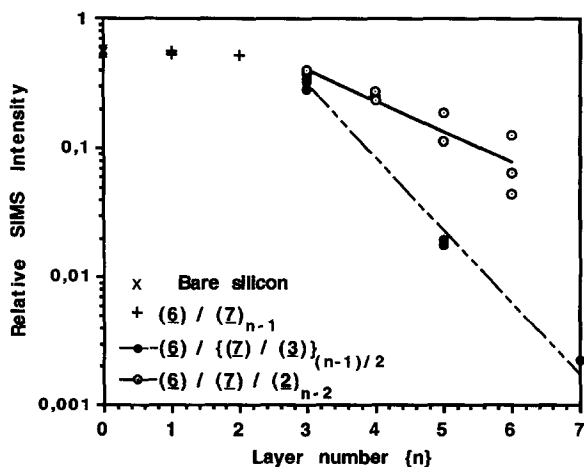


Fig. 3. Relative intensity of the  $\text{Si}^+$  substrate ion as a function of the layer number ( $n$ ) for two types of assembly,  $(6)/(7)/(3)_x$  and  $(6)/(7)/(2)_x$ .

### 3.2.1. SIMS-XRR correlation

In Fig. 4 the X-ray reflectivity is displayed versus the component of the photon wavevector perpendicular to the interfaces ( $K_{z0}$ ) for the assemblies  $(6)/(7)/(2)_x$  ( $x=1,2$ ) and  $(6)/(7)/(3)_x$  ( $x=2,3$ ). For samples based on polycation (3), the overall thickness was obtained from the spacing of the Kiessig fringes  $((6)/(7)/(3)_2:88 \text{ \AA}$  and  $(6)/(7)/(3)_3:111 \text{ \AA}$ ). In addition to the Kiessig fringes, Bragg peaks corresponding to a repetition distance of  $25 \text{ \AA}$  were also observed in the reflectivity (Fig. 4c and d, resulting from the internal structure of the multilayers). A more detailed analysis of these curves is presented elsewhere [16]. For samples  $(6)/(7)/(2)_x$  ( $x=1,2$ ), the Kiessig fringes are more damped due to higher

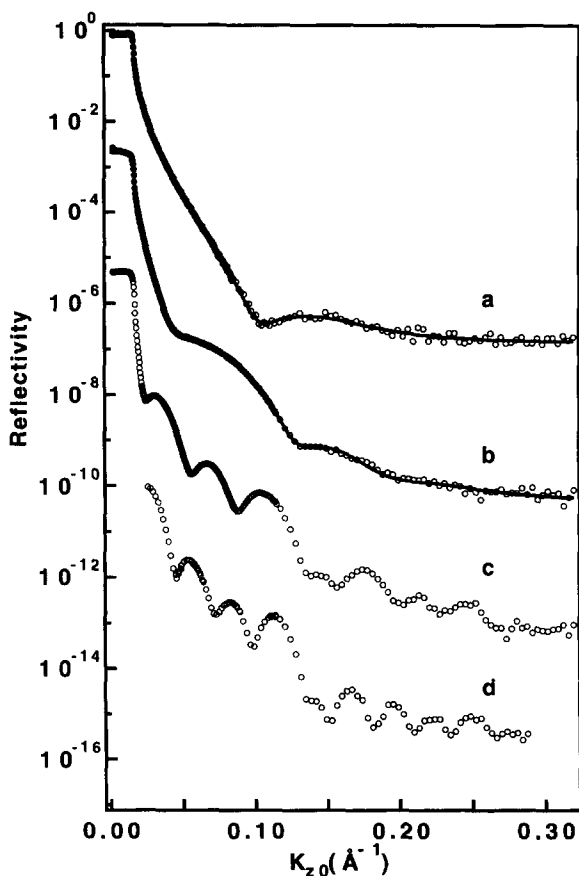


Fig. 4. X-ray reflectivity versus the component of the photon wavevector perpendicular to the interfaces ( $K_{z0}$ ), and best fits to the data. The points are shifted vertically for clarity. The formulations of the assemblies analyzed are (a):  $(6)/(7)/(2)_1$ , (b):  $(6)/(7)/(2)_2$ , (c):  $(6)/(7)/(3)_2$ , and (d):  $(6)/(7)/(3)_3$ .

interfacial roughness, and a more detailed analysis is required. A matrix iterative formalism derived from Fresnel's equations [17], including effects due to roughness [18], was used to fit the experimental data, allowing the extraction of the electron density profiles perpendicular to the substrates (Figs. 4 and 5). The thicknesses of the multilayers were then obtained from the density profiles, by computing the distances between the maxima of the first derivatives of the profiles versus distance. Values of  $13 \text{ \AA}$  and  $37 \text{ \AA}$  were obtained for the assemblies  $(6)/(7)/(2)_1$  and  $(6)/(7)/(2)_2$ , respectively. These numbers represent the effective thickness of the multilayers, i.e. the thickness of a hypothetical film of zero roughness containing the same amount of polymer as the real film.

Fig. 6 shows the correlation between the inten-

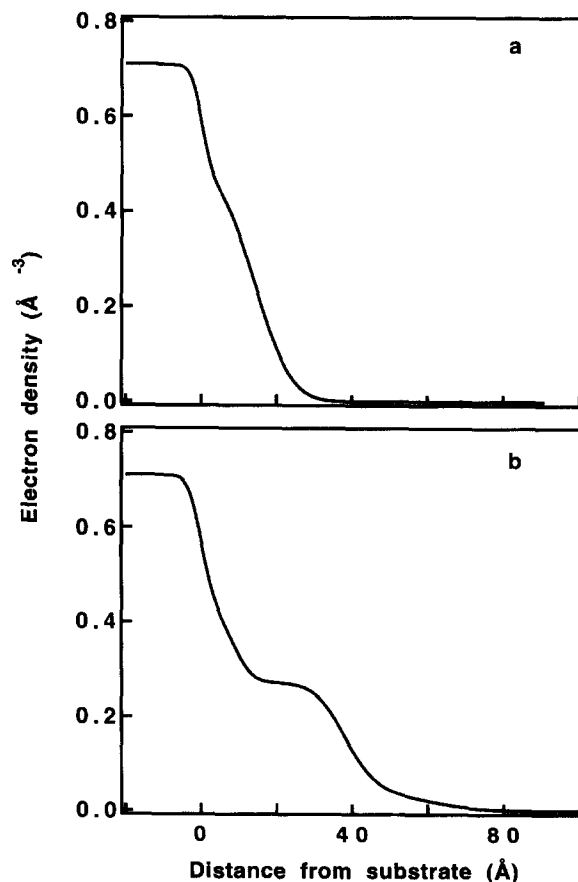


Fig. 5. Electron density profiles computed from the data of Fig. 4 for the assemblies (a):  $(6)/(7)/(2)_1$  and (b):  $(6)/(7)/(2)_2$ .

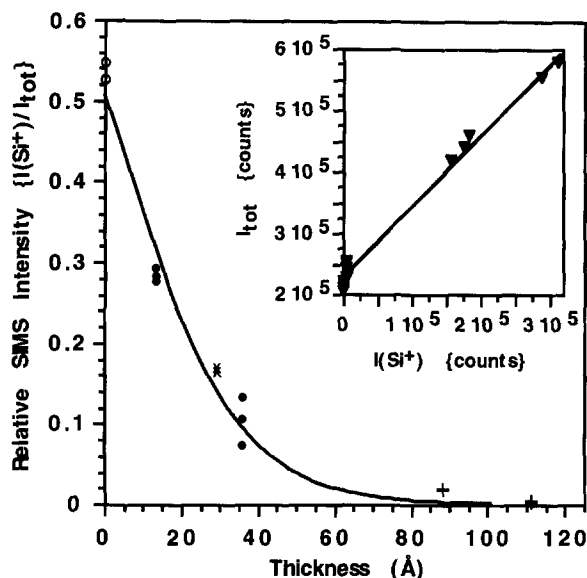


Fig. 6. Relative intensity of the  $\text{Si}^+$  substrate ion as a function of the film thickness for three types of assemblies and for a cleaned silicon wafer. The open circle ( $\circ$ ) refers to the clean silicon wafer, the full circle ( $\bullet$ ) to the assemblies  $(6)/(7)/(2)_x$  ( $x=1,2$ ), the cross ( $\times$ ) to the assembly  $(6)/(7)/(5)_2$  and the plus ( $+$ ) to the assemblies  $(6)/(7)/(3)_x$  ( $x=2,3$ ). The thickness is measured by XRR, except in the case of the assembly  $(6)/(7)/(5)_2$ , where it is measured by AFM. The inset shows the linear relation between the  $\text{Si}^+$  signal and the total intensity.

sity of the  $\text{Si}^+$  signal, normalized to the total spectrum intensity, and the thickness of the multilayer assembly measured by XRR in most cases, or by AFM (assembly  $(6)/(7)/(5)_2$ ). The full line in Fig. 6 relates to a model of exponential decay of the substrate SI intensities as a function of the thickness of the organic layer ( $I = I^0 \exp(-d/\lambda)$ ). It must be mentioned that the relation between the total intensity and the  $\text{Si}^+$  intensity is linear for this set of samples ( $I_{\text{tot}} = 1.16I(\text{Si}^+) + 2.28 \times 10^5$ ), which explains the form of the law modeling the data in Fig. 6:  $I(\text{Si}^+)/I_{\text{tot}} = \exp(-x/\lambda(\text{Si}^+)) / [1.16 \exp(-x/\lambda(\text{Si}^+)) + 2.28 \times 10^5 / I^0]$ . In this fit, the value of  $I^0$  is equal to  $2.82 \times 10^5$  and the mean emission depth of the  $\text{Si}^+$  ion,  $\lambda(\text{Si}^+)$ , is 14.8 Å. The good correlation of the data suggests that the exact formulation of the multilayered sample is not relevant in this case. Nevertheless, it is important to note that this value of the mean emission depth  $\lambda$  is valid only for a uniform coverage of the sample (thickness  $d$ ).

### 3.2.2. SIMS-XPS correlation

**3.2.2.1. Theoretical considerations.** Let us examine the general case of a coverage with a non-uniform thickness, assuming for the SIMS intensity an exponential decay as a function of thickness for the substrate atoms. The analyzed area can be divided in  $n$  sub-areas  $S_i$  of thickness  $d_i$ . So, for ion  $j$ , the total intensity  $I_j$  can be written:

$$I_j = I_j^0 \sum (S_i/S) \exp(-d_i/\lambda_j), \quad (1)$$

where  $S = \sum S_i$ . The intensity ratio  $I_j/I_k$  is given by:

$$I_j/I_k = (I_j^0/I_k^0) [\sum S_i \exp(-d_i/\lambda_j)] / [\sum S_i \exp(-d_i/\lambda_k)]. \quad (2)$$

This equation can be simplified in three cases at least: (i) The mean emission depths  $\lambda_{j,k}$  are equal; Eq. (2) then describes a linear relationship between  $I_j$  and  $I_k$ . (ii) The sample is partially covered ( $d_1=0$ ) and the thicknesses  $d_i$  ( $i>1$ ) are great compared to the mean emission depths  $\lambda_{j,k}$  (which means that the effect of the emission depth is negligible). Once more, the ratio  $I_j/I_k$  is constant. (iii) The film thickness is uniform; Eq. (2) then becomes:

$$I_j/I_k = (I_j^0/I_k^0) \exp[-d/(\lambda_j - \lambda_k)]. \quad (3)$$

In the case of uniform thickness,  $I_k$  can also be written as a function of  $I_j$ :

$$I_k = (I_k^0/I_j^0)^{\lambda_j/\lambda_k} I_j^{\lambda_j/\lambda_k} \quad (4)$$

This equation shows that in the case of uniform coverage, the correlation between the intensities of substrate ions having different mean emission depths can be described by a power law.

**3.2.2.2. Experimental data.** A first set of XPS measurements was done at the usual angle of detection ( $35^\circ$  with respect to the sample surface). For each sample, detailed scans of the C 1s, O 1s, N 1s, S 2p and Si 2p lines were recorded. A Shirley-type non-linear background subtraction was used [19], and the peaks were decomposed by using a least square routine assuming a Gaussian/Lorentzian (85/15) function. The XPS atomic percentages (Table 6) were calculated from the peak area of each element, corrected by the

Table 6

XPS atomic percentage of the elements for two types of assemblies, (6)/(7)/(2)<sub>x</sub> and (6)/(7)/(3)<sub>x</sub>. (Si–Si) refers to the crystalline silicon component and (Si–O<sub>x</sub>) to the oxide component of the Si 2p line; the mean binding energies of the different element lines in these samples are C 1s: 284.8 eV(C–C), O 1s: 532.8 eV, N 1s: 401.0 eV, S 2p: 168.8 eV and Si 2p: 98.5 eV(Si–Si) and 102.5 eV(Si–O<sub>x</sub>)

Sample	XPS atomic percentage					
	C	O	N	S	Si-Si	Si-O <sub>x</sub>
(6)	21.1	37.1	–	7.5	27.1	7.2
(6)/(7)	20.1	38.0	–	7.5	27.0	7.4
(6)/(7)/(2)	25.5	38.0	1.9	5.0	20.9	8.7
(6)/(7)/(2) <sub>2</sub>	45.7	29.8	3.9	3.1	12.1	5.4
(6)/(7)/(2) <sub>3</sub>	55.3	26.2	4.1	2.7	5.8	5.9
(6)/(7)/(2) <sub>4</sub>	60.4	24.8	5.2	2.5	3.1	3.9
(6)/(7)/(3)	35.9	26.5	3.0	4.7	21.9	8.0
(6)/(7)/(3) <sub>2</sub>	68.4	19.8	6.8	2.2	2.1	0.7
(6)/(7)/(3) <sub>3</sub>	70.7	18.9	7.0	2.3	0.7	0.4
(6)/(7)/(3) <sub>4</sub>	69.1	19.9	6.2	2.5	1.5	0.8

corresponding sensitivity factor (C 1s: 1.0, O 1s: 2.49, N 1s: 1.68, S 2p: 1.79 and Si 2p: 0.90). Two series of samples are considered in Table 6 ((6)/(7)/(3)<sub>x</sub> and (6)/(7)/(2)<sub>x</sub>). The Si 2p line is decomposed in its two components, attributed to pure crystalline silicon (Si–Si) and to silicon oxide (Si–O<sub>x</sub>). The ratio of this two components ((Si–O<sub>x</sub>)/(Si–Si)) is lower than 0.6 except in two cases ((6)/(7)/(2)<sub>3</sub>:1.0 and (6)/(7)/(2)<sub>4</sub>:1.3). For these samples, ToF-SIMS has shown that some poly(dimethyl siloxane) contamination occurred. Consequently, these data are not used for the ToF-SIMS sampling depth determination. As expected, the increase of the carbon and the decay of the silicon percentages are correlated. Moreover, the comparison with the ToF-SIMS data (Fig. 3) allows us to confirm the conclusions drawn in Section 3.1.4 for these assemblies. The high (Si–Si) percentage observed for the assembly (6)/(7)/(3) suggests in addition that the deposition of the first polycation (3) layer in this system is problematic.

For the substrate signal, the correlation between XPS and ToF-SIMS data is very good in the case of the assemblies (6)/(7)/(3)<sub>x</sub> and (6)/(7)/(2)<sub>x</sub>. The best correlation, shown in Fig. 7a, is obtained between the Si<sup>+</sup> SI signal and the Si 2p (Si–Si) component. The inset shows the striking linear correlation obtained when the data are normalized

(SIMS  $I(\text{Si}^+)/I(\text{tot})$  versus XPS Si 2p (Si–Si) atom%). According to the theoretical considerations, the good correlation between SIMS and XPS values is in agreement with a SI mean emission depth following Eq. (4), with  $I_{\text{SIMS}} = KI_{\text{XPS}}^{\lambda_{\text{XPS}}/\lambda_{\text{SIMS}}}$ . As SIMS imaging and other characterization techniques (XRR, AFM) do not indicate a lateral alternation of zones covered by the polyelectrolyte and uncovered zones (bare silicon), an explanation of the correlation based solely on the inhomogeneity of the coverage can be excluded. Another argument is related to Fig. 7b and c. They present the relative intensities of the SiOH<sup>+</sup> and SiO<sub>3</sub>H<sup>−</sup> ions as a function of the Si<sup>+</sup> ion relative intensity. The data can be fitted by a power law too. In the case of an incomplete coverage, with substrate ions coming from the bare silicon zones only, the relation between different substrate ion intensities, as well the relation between SIMS and XPS intensities (Fig. 7a, should be linear (see theoretical section). As this is obviously not the case, an effect of the emission depth must be considered.

For a uniform coverage, the curve shapes in Figs. 7a, b and c can be explained by different values of the mean emission depth. Indeed, if  $I(\text{Si 2p}) = I^0(\text{Si 2p}) \exp[-d/\lambda(\text{Si 2p})]$ ,  $I(\text{Si}^+) = I^0(\text{Si}^+) \exp[-d/\lambda(\text{Si}^+)]$ ,  $I(\text{SiOH}^+) = I^0(\text{SiOH}^+) \exp[-d/\lambda(\text{SiOH}^+)]$  and  $I(\text{SiO}_3\text{H}^-) = I^0(\text{SiO}_3\text{H}^-) \exp[-d/\lambda(\text{SiO}_3\text{H}^-)]$ , one obtains according to Eq. (4):

$$I(\text{Si}^+) = KI(\text{Si 2p})^{\lambda(\text{Si 2p})/\lambda(\text{Si}^+)}, \quad (5)$$

$$I(\text{SiOH}^+) = K'I(\text{Si}^+)^{\lambda(\text{Si}^+)/\lambda(\text{SiOH}^+)}, \quad (6)$$

$$I(\text{SiO}_3\text{H}^-) = K''I(\text{Si}^+)^{\lambda(\text{Si}^+)/\lambda(\text{SiO}_3\text{H}^-)}, \quad (7)$$

where  $K$  is independent of  $I(\text{Si 2p})$ , and  $K'$ ,  $K''$  are independent of  $I(\text{Si}^+)$ . From the fitting of the curves in Fig. 7, we find  $\lambda(\text{Si 2p})/\lambda(\text{Si}^+) = 1.9$ ,  $\lambda(\text{Si}^+)/\lambda(\text{SiOH}^+) = 1.9$  and  $\lambda(\text{Si}^+)/\lambda(\text{SiO}_3\text{H}^-) = 3.1$ . Empirical and experimental relations giving the mean free path of the photoelectrons into the matter can be found in the literature [20–23]. Following the well-known empirical relationship of Seah and Dench (SD),  $\lambda = 1/\rho(0.49/E^2 + 0.11E^{0.5})$  [20], a value of 47 Å is obtained for  $\lambda(\text{Si 2p})$ . In comparison, using the empirical law of Roberts et al. (R),  $\lambda = KE^{1.2}$  [22],

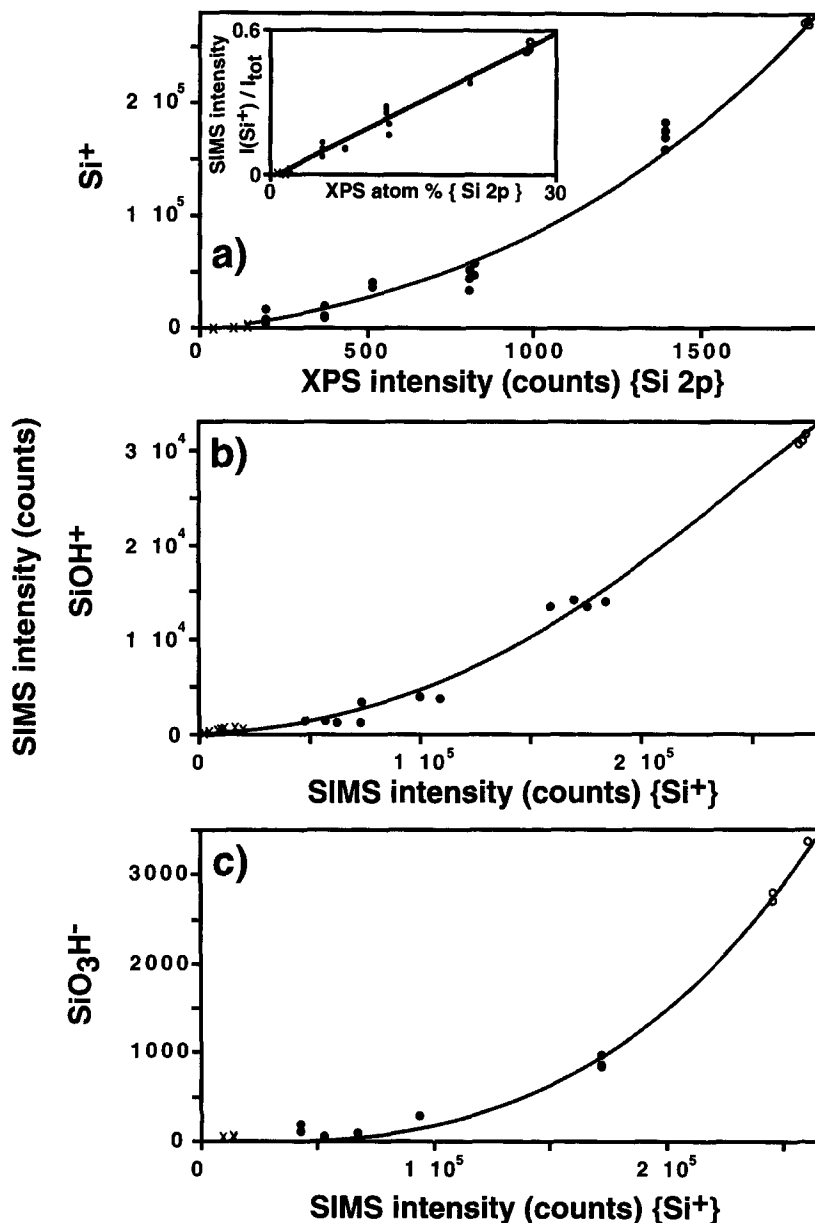


Fig. 7. (a) Correlation between the *absolute*  $\text{Si}^+$  SI intensity and XPS Si 2p intensity (Si–Si). The open circle ( $\circ$ ) refers to the assemblies (6) and (6)/(7), the full circle ( $\bullet$ ) to the assemblies (6)/(7)/(1) and (6)/(7)/(2)<sub>x</sub> ( $x=1,2$ ), and the cross (x) to the assemblies (6)/(7)/(3)<sub>x</sub> ( $x=2-4$ ). The inset shows the linear correlation between the *relative* intensity of  $\text{Si}^+$  and the XPS atom percentage of Si. (b) Correlation between the absolute  $\text{SiOH}^+$  and  $\text{Si}^+$  SI intensities. (c) Correlation between the absolute  $\text{SiO}_3\text{H}^-$  and  $\text{Si}^+$  SI intensities.

valid for PMMA, one obtains for the Si 2p line a value of 31 Å. The mean emission depth of the secondary ion  $\text{Si}^+$  would then be  $47 \sin(35^\circ)/1.9 = 14.2$  Å or  $31 \sin(35^\circ)/1.9 = 9.3$  Å, respectively. The first value is close to the 14.8 Å found in

Section 3.2.1, whereas the second is significantly lower. Also in the hypothesis of the uniform coverage, the mean emission depth is equal to 7.5 Å (SD) or 4.9 Å (R) for  $\text{SiOH}^+$  and to 4.6 Å (SD) or 3.0 Å (R) for  $\text{SiO}_3\text{H}^-$  (Eq. (6) Eq. (7)).

For a coverage with non-uniform thickness, a more complex treatment is needed.

Angle resolved XPS measurements were also realized on four assemblies in order to confirm the

values given above. Fig. 8 reports the XPS Si 2p intensities at 15°, 25° and 35° as a function of the SI intensities of Si<sup>+</sup>, SiOH<sup>+</sup> and SiO<sub>3</sub>H<sup>-</sup> (Fig. 8a, b and c respectively). In Fig. 8a the relationship

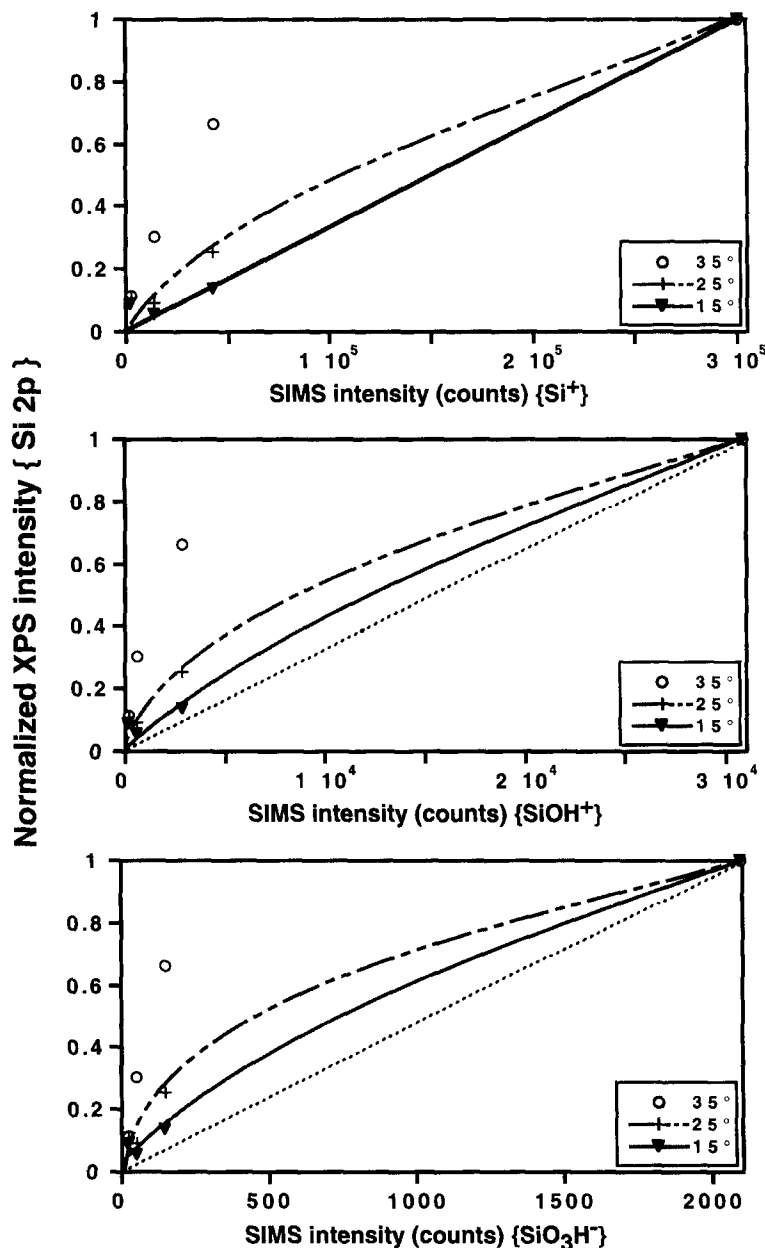


Fig. 8. (a) Correlation between the XPS Si 2p absolute intensity at different angles (15°, 25°, 35°) and the Si<sup>+</sup> SI absolute intensity for 4 samples {cleaned silicon, assembly (6)/(7)/(2)<sub>x</sub> (x=2,3), assembly (6)/(7)/(3)<sub>2</sub>}. The SI intensities are mean values (3 values at least). (b) Correlation between the XPS Si 2p absolute intensity at different angles and the SiOH<sup>+</sup> SI absolute intensity. (c) Correlation between the XPS Si 2p absolute intensity at different angles and the SiO<sub>3</sub>H<sup>-</sup> SI absolute intensity.

which is the closest to linearity is obtained between Si 2p (15°) photoelectrons and Si<sup>+</sup> SI ions, and the deviation from linearity grows when the XPS angle increases. The linear correlation between the SIMS Si<sup>+</sup> data and the XPS Si 2p (15°) data allows us to deduce the Si<sup>+</sup> mean emission depth ( $\lambda$ ) from the simple equation  $\lambda_{\text{SIMS}} = \lambda_{\text{XPS}} \sin(15^\circ)$ . This indicates a mean emission depth of 12.2 Å (SD) or 8.0 Å (R), which constitutes a lower limit to the values calculated above. It is important to keep in mind that the  $\lambda$  value obtained from the linear regression does not depend on the coverage quality and roughness (see theoretical section). This value of  $\lambda$  is some 15% lower than those obtained assuming a uniform thickness of the sample. Considering the limited accuracy of the method, this is not sufficient to determine whether the layer is uniform or not.

Fig. 8b shows that, even for an angle of detection of 15° in XPS, the deviation from linearity in the correlation between XPS and SIMS data is marked for the SiOH<sup>+</sup> ion, in agreement with a lower mean emission depth of this ion. In addition, the deviation increases with the size of the secondary ion considered (SiO<sub>3</sub>H<sup>-</sup>; Fig. 8c).

#### 4. Conclusion

ToF-SIMS offers valuable information concerning the quality of thin polymeric coatings such as polyelectrolyte multilayered assemblies. By imaging the spatial distribution of the secondary ions, the nature and homogeneity of the surface can be verified on a local scale. The sensitivity to the sample thickness in the case of very thin films (some nanometers), related to the attenuation depth of the substrate ions in the organic film, provides another tool to evaluate the sample quality. As shown by the correlation with other techniques (XRR, XPS, AFM), the information given by the substrate ions is quantitative.

In a more fundamental way, the mean free path of several secondary ions (Si<sup>+</sup>, SiOH<sup>+</sup>, SiO<sub>3</sub>H<sup>-</sup>) in the organic film has been determined by the correlation with XRR and XPS data. Assuming an exponential decay of the ion intensities as the thickness of the assembly increases, our model

shows that the mean free path is reduced by a factor of 2 when going from Si<sup>+</sup> to SiOH<sup>+</sup> and by a factor of 3 when going from Si<sup>+</sup> to SiO<sub>3</sub>H<sup>-</sup>. This suggests more generally that atomic or small molecular ions are less surface sensitive than large molecular ions.

Finally, this work suggests that the study of the polyelectrolyte assemblies by the combination of several complementary techniques, leading to a more fundamental understanding both of the deposition process and of the characterization techniques themselves, is the best way to improve the quality and reproducibility of polyelectrolyte thin film deposition in the future.

#### Acknowledgements

Dr. B. Nysten is gratefully acknowledged for the AFM measurements. This work and three of us (A.D., X.A. and E.W.) are supported by the “Action de Recherche Concertée” (94/99-173) of the “Communauté Française de Belgique, Direction Générale de l’Enseignement Supérieur et de la Recherche Scientifique”. Partial financial support was also provided by the Belgian National Fund for Scientific Research (A.J.). The ToF-SIMS equipment was acquired with the support of the “Région Wallonne” and “FRFC-Loterie Nationale” of Belgium.

#### References

- [1] G. Decher, J.D. Hong and J. Schmitt, *Thin Solid Films* 210/211 (1992) 831.
- [2] J. Schmitt, T. Grünwald, G. Decher, P.S. Pershan, K. Kjaer and M. Lösche, *Macromolecules* 26 (1993) 7058.
- [3] Y. Lvov, K. Ariga, I. Ichinose and T. Kunitake, *J. Am. Chem. Soc.* 117 (1995) 6117.
- [4] A. Laschewsky, B. Mayer, E. Wischerhoff, X. Arys and A. Jonas, *Ber. Bunsenges. Phys. Chem.*, to be published.
- [5] G. Bolbach, R. Beavis, S. Della-Negra, C. Deprun, W. Ens, Y. Lebeyec, D.E. Main, B. Schueler and K.G. Standing, *Nucl. Instrum. Methods B* 30 (1988) 74.
- [6] B. Hagenhoff, M. Deimel, A. Benninghoven, H-U. Siegmund and D. Holtkamp, *J. Phys. D* 25 (1992) 818.
- [7] R.W. Johnson Jr., J. Li, P.A. Cornelio-Clark, and J.A. Gardella Jr., in: *Secondary Ion Mass Spectrometry, SIMS*

- VIII, Eds. A. Benninghoven, K.T.F. Janssen, J. Tümpner, H.W. Werner (Wiley, New York, 1992) p. 293.
- [8] P. Hendlinger, A. Laschewsky, P. Bertrand, A. Delcorte, R. Legras, B. Nysten and D. Möbius, abstract presented at the Seventh International Conference on Organized Molecular Films (Ancona, September 1995).
- [9] A. Laschewsky, B. Mayer, E. Wischerhoff, X. Arys, A. Jonas, P. Bertrand and A. Delcorte, presented at the Seventh International Conference on Organized Molecular Films (Ancona, September 1995); accepted for *Thin Solid Films*.
- [10] A. Laschewsky, E. Wischerhoff and B. Mayer, to be published.
- [11] B.W. Schueler, *Microsc. Microanal. Microstruct.* 3 (1992) 119.
- [12] A. Delcorte, L.T. Weng and P. Bertrand, *Nucl. Instrum. Meth. B* 100 (1995) 213.
- [13] L.T. Weng, G. Vereecke, M.J. Genet, P. Bertrand and W.E.E. Stone, *Surf. Interface Anal.* 20 (1993) 179.
- [14] L.T. Weng, G. Vereecke, M.J. Genet, P.G. Rouxhet, J.H. Stone-Masui, P. Bertrand and W.E.E. Stone, *Surf. Interface Anal.* 20 (1993) 193.
- [15] M.P. Seah, in: *Practical Surface Analysis by Auger and X-ray Photoelectron Spectroscopy*, Eds. D. Briggs and M.P. Seah (Wiley, New York, 1983) p. 181.
- [16] X. Arys and A. Jonas, presentation at the March Meeting of the American Physical Society, St Louis (1996).
- [17] J. Lekner, *Theory of Reflection* (Nijhoff, Dordrecht, 1987).
- [18] S.K. Sinha, E.B. Sirota, S. Garoff and H.B. Stanley, *Phys. Rev. B* 38 (1988) 2297.
- [19] D.A. Shirley, *Phys. Rev. B* 5 (1972) 4709.
- [20] M.P. Seah and W.A. Dench, *Surf. Interface Anal.* 1 (1979) 2.
- [21] C.D. Wagner, W.M. Riggs, L.E. Davis, J.F. Moulder and G.E. Muilenberg, *Handbook of X-Ray Photoelectron Spectroscopy* (Perkin-Elmer Corporation, 1979).
- [22] R.F. Roberts, D.L. Allara, C.A. Pyrd, D.N.E. Buchanan and N.D. Hobbs, *Surf. Interface Anal.* 2 (1980) 5.
- [23] T.J. Horr, J. Ralston, R.St.C. Smart, *Colloids Surfaces A* 92 (1994) 277.